Variability of surface water characteristics and Heinrich-like events in the Pleistocene midlatitude North Atlantic Ocean: Biomarker and XRD records from IODP Site U1313 (MIS 16–9)

Ruediger Stein,[1] Jens Hefter,[1] Jens Grützner,[2] Antje Voelker,[3] and B. David A. Naafs[1,4]

Received 28 April 2008; revised 9 February 2009; accepted 23 February 2009; published 1 May 2009.

[1] A reconstruction of Milankovitch to millennial-scale variability of sea surface temperature (SST) and sea surface productivity in the Pleistocene midlatitude North Atlantic Ocean (marine isotope stage (MIS) 16–9) and its relationship to ice sheet instability was carried out on sediments from Integrated Ocean Drilling Program (IODP) Site U1313. This reconstruction is based on alkenone and *n*-alkane concentrations, $U^{K'}_{37}$ index, total organic carbon (TOC) and carbonate contents, X-ray diffraction data, magnetic susceptibility, and accumulation rates. Increased input of ice-rafted debris occurred during MIS 16, 12, and 10, characterized by high concentrations of dolomite, quartz, and feldspars and elevated accumulation rates of terrigenous matter. Minimum input values of terrigenous matter, on the other hand, were determined for MIS 13 and 11. Peak values of dolomite, coinciding with quartz, plagioclase, and kalifeldspar peaks and maxima in long-chain *n*-alkanes indicative for land plants, are interpreted as Heinrich-like events related to sudden instability of the Laurentide Ice Sheet during early and late (deglacial) phases of the glacials. The coincidence of increased TOC values with elevated absolute concentrations of alkenones suggests increased glacial productivity, probably due to a more southern position of the Polar Front. Alkenone-based SST reached absolute maxima of about 19°C during MIS 11.3 and absolute minima of <10°C during MIS 12 and 10. Within MIS 11, prominent cooling events (MIS 11.22 and 11.24) occurred. The absolute SST minima recorded directly before and after the glacial maxima MIS 10.2 and 12.2 are related to Heinrich-like event meltwater pulses, as supported by the coincidence of SST minima and maxima in $C_{37:4}$ alkenones and dolomite. These sudden meltwater pulses, especially during terminations IV and V, probably caused a collapse of phytoplankton productivity as indicated by the distinct drop in alkenone concentrations. Ice sheet disintegration and subsequent surges and outbursts of icebergs and meltwater discharge may have been triggered by increased insolation in the northern high latitudes.

Citation: Stein, R., J. Hefter, J. Grützner, A. Voelker, and B. D. A. Naafs (2009), Variability of surface water characteristics and Heinrich-like events in the Pleistocene midlatitude North Atlantic Ocean: Biomarker and XRD records from IODP Site U1313 (MIS 16–9), *Paleoceanography*, *24*, PA2203, doi:10.1029/2008PA001639.

1. Introduction and Objectives

[2] Understanding the mechanisms and causes of abrupt climate change is one of the major challenges in paleoclimate research today. In marine sediment cores from the North Atlantic, these climate changes are manifested by the so-called "Heinrich events" [e.g., *Bond et al.*, 1992, 1999; *Broecker et al.*, 1992; *Andrews et al.*, 1993; *Broecker*, 1994; *Bond and Lotti*, 1995; *Stoner et al.*, 1996; *Kissel et al.*, 1999; *Sarnthein et al.*, 2001] (see *Hemming* [2004] for review). Heinrich events are characterized by major input of ice-rafted debris (IRD) and meltwater pulses, documenting episodes of sudden instability and collapse of the Laurentide-Greenland Ice Sheet during the last glacial period.

[3] Heinrich events and Heinrich layers first found by *Heinrich* [1988] in sediment cores from the eastern North Atlantic, occur in a band across the northern North Atlantic at about 40–65°N, approximately coinciding with the North Atlantic Current and the IRD belt of *Ruddiman* [1977] (Figure 1). The Heinrich layers display an increase in terrigenous coarse-grained IRD, a low abundance of foraminifers, and a prominent presence of detrital limestone and dolomite [*Andrews and Tedesco*, 1992; *Bond et al.*, 1992, 1999; *Broecker et al.*, 1992; *Andrews et al.*, 1993, 1994; *Grousset et al.*, 1993; *Bond and Lotti*, 1995; *Dowdeswell et al.*, 1995; *van Kreveld et al.*, 1996; *Kirby and Andrews*, 1999; *Rashid et al.*, 2003] (see *Hemming* [2004] for review). The high concentration of detrital carbonates indicates that the carbonate-bearing icebergs originated in the Hudson Strait and adjacent shelf regions. The absence of the carbonate-rich layers south of the IRD belt [*Ruddiman*, 1977] suggests that rapid melting of icebergs occurred before they reached the warmer water south of the glacial Polar Front [*Ruddiman*, 1977; *Bond et al.*, 1992]. Within the

[1]Alfred Wegener Institute for Polar and Marine Research, Bremerhaven, Germany.
[2]Center for Marine Environmental Sciences, Bremen University, Bremen, Germany.
[3]Departamento Geologia Marinha, LNEG, Alfragide, Portugal.
[4]Institute for Geosciences, Potsdam University, Potsdam, Germany.

0883-8305/09/2008PA001639

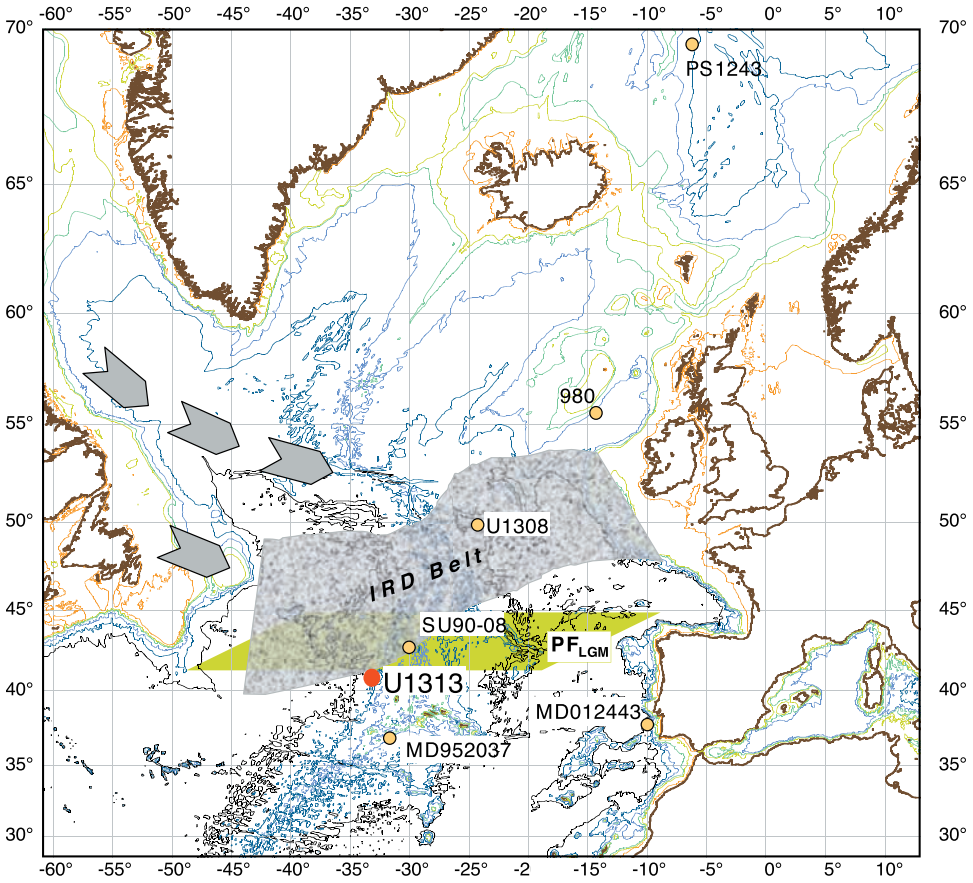

Figure 1. Map with locations of IODP Site U1313 [*Channell et al.*, 2006] and further cores discussed in the text. In addition, *Ruddiman's* [1977] IRD belt and postulated location of the Last Glacial Maximum Polar Front (PF_{LGM}) [*Pflaumann et al.*, 2003].

IRD belt of *Ruddiman* [1977], Heinrich layers are most clearly identifiable also in anomalously high magnetic susceptibility values [e.g., *Grousset et al.*, 1993; *Robinson et al.*, 1995]. Furthermore, the layers were identified by specific organic carbon compounds such as odd-numbered long-chain *n*-alkanes as indicator for higher land plants [e.g., *Madureira et al.*, 1997; *Rosell-Melé et al.*, 1997; *Villanueva et al.*, 1997].

[4] The low abundance of planktonic foraminifers found in Heinrich layers probably resulted from either a distinct decrease in surface water productivity or dilution due to significantly increased supply of IRD [*Broecker et al.*, 1992; *van Kreveld et al.*, 1996; *McManus et al.*, 1998]. Within these layers, *Neogloboquadrina pachyderma* sinistral is the dominant planktonic foraminiferal species [e.g., *Heinrich*, 1988; *Bond et al.*, 1992; *Broecker et al.*, 1992], indicating an increase in the penetration of polar (melt) water into the North Atlantic around 50°N [e.g., *Bond et al.*, 1992; *Maslin et al.*, 1995]. This may reflect a decrease in both sea surface temperature and salinity during these intervals [e.g., *Bond et al.*, 1992; *Broecker et al.*, 1992], as also supported by alkenone data [e.g., *Madureira et al.*, 1997; *Rosell-Melé et al.*, 1997, 2002; *Bard et al.*, 2000; *Calvo et al.*, 2001; *Rosell-Melé*, 2001] (see sections 5.2 and 5.3).

[5] Whereas most of the high-resolution records dealing with Heinrich events and climate change are concentrating on the last glacial/interglacial cycle, here we present new data from Integrated Ocean Drilling Program (IODP) Site U1313 representing the time interval of 320–640 ka. Site U1313, a reoccupation of DSDP Site 607 [e.g., *Ruddiman et al.*, 1987, 1989; *Raymo et al.*, 1989], is located at the base of the western flank of the Mid-Atlantic Ridge in a water depth of 3426 m, ~240 miles northwest of the Azores and within Ruddiman's IRD belt (Figure 1) [*Channell et al.*, 2006; *Stein et al.*, 2006]. With these new U1313 records, we are able to compare IRD deposition and surface water temperature, salinity, and productivity in the central North Atlantic within the IRD belt during very different glacial and interglacial intervals, i.e., on one hand the more severe glacials marine isotope stage (MIS) 10, MIS 12, and MIS 16, and the weaker MIS 14, and, on the other hand, the extreme interglacial MIS 11 and the less extreme interglacials MIS 13 and MIS 15.

2. Methods

[6] X-ray diffraction (XRD), carbonate, organic carbon, and biomarker analyses were carried out at the Alfred Wegener Institute (AWI) on the same set of samples taken

from the U1313 primary splice (see supplementary data at http://dx.doi.org/10.1594/PANGAEA.712917).[1]

[7] For identifying ice rafting in the northern North Atlantic, siliciclastic (terrigenous) minerals (i.e., quartz and feldspars) were determined by XRD [see *Moros et al.*, 2004]. For XRD measurements of samples from Site U1313, a split of 1–2 g of ground bulk sediment was measured continuously using a Phillips PW3020 diffractometer equipped with cobalt kα radiation, automatic divergence slit, graphite monochromator, and automatic sample changer. For the purposes of this study, a spectrum from 20 to 40° 2Theta, which involves the major peaks of quartz (3.34 Å, 4.26 Å), kalifeldspar (3.23 Å), plagioclase (3.19 Å), calcite (3.04 Å), and dolomite (2.89 Å), was used. Data are presented as relative intensity values. Because the 3.34 Å peak may also belong to other minerals (e.g., illite), for further evaluation the quartz peak at 4.26 Å (generally about 35% of the intensity of the most intense peak at 3.34 Å) was used. XRD measurements were carried out on 880 samples of the interval 14–32 m composite depth (mcd), representing the time interval of about 320–640 ka, which gives a time resolution of about 360 years.

[8] The determination of total carbon (TC) and total organic carbon (TOC) as basic parameters were performed on all samples by LECO technique. The carbonate content was calculated as

$$CaCO_3 = (TC - TOC) * 8.334$$

assuming that calcite is the predominant carbonate phase. This assumption is supported by calcite/(calcite + dolomite) XRD intensity ratios of >0.98; only in a restricted number of samples with dolomite peaks the ratio may decrease to values between 0.97 (MIS 12) and 0.85 (MIS 16).

[9] In order to get information about the marine and terrigenous proportions of the organic carbon fraction in marine sediments, (1) the long-chain C_{27}, C_{29}, and C_{31} *n*-alkanes as indicator for land-derived vascular plant material [e.g., *Prahl and Muehlhausen*, 1989; *Villanueva et al.*, 1997], and (2) the alkenones mainly synthesized by marine coccolithophorids and indicative for marine surface water productivity [*Volkman et al.*, 1980; *Marlowe et al.*, 1984, 1990; *Conte et al.*, 1992; *Müller et al.*, 1998; *Villanueva et al.*, 2001], were determined by means of gas chromatography/time-of-flight mass spectrometry (GC/TOFMS).

[10] After freeze-drying and homogenization, batches of 24 samples were weighed into stainless steel extraction cells, using about 3–6 g of sediment per individual sample, and extracted with dichloromethane by accelerated solvent extraction (ASE 200, DIONEX, 5 min. at 100°C and 1000 psi) following an approved protocol known to be suitable to extract the targeted compound classes [*Calvo et al.*, 2003]. For quantification purposes, 2.1435 μg of *n*-hexatriacontane (*n*-C_{36} alkane, obtained from Sigma-Aldrich/Fluka) was added as internal standard to each sample prior to extraction. Excess solvent was removed by rotary evaporation, samples were transferred to autosampler vials and redissolved in 1 mL hexane prior to analyses by fast GC/TOFMS.

[11] The GC/TOFMS system used consisted of a Leco Pegasus III (Leco Corp., St. Joseph, MI) interfaced to an Agilent 6890 GC. The gas chromatograph was equipped with a 10 m long by 0.18 mm in diameter Rtx-1MS (Restek Corp.) column (film thickness: 0.10 μm) and a temperature programmable cooled injection system (CIS4, Gerstel) in combination with an automated liner exchange facility (Alex, Gerstel) and a multipurpose autosampler (MPS 2, Gerstel).

[12] A series of alkenone standards and reference mixtures of known $U^{K}_{37}{}'$ values was used to determine linear response factor equations for quantification of alkenones in the studied samples and to convert GC/TOFMS specific $U^{K}_{37}{}'$ values into appropriate GC/FID equivalents. Full details on the calibration and conversion routines necessary for alkenone analysis by GC/TOFMS are given by *Hefter* [2008]. Concentrations of *n*-alkanes were determined from GC/TOFMS peak areas integrated on mass (*m*/*z*) 71, whereby compound specific response factors have been obtained from calibration with an external *n*-alkane standard (Chiron AS, Norway).

[13] The alkenone-based approach was used to reconstruct sea surface water temperatures (SST). This method evolved from the observation that certain microalgae of the class *Prymnesiophyceae*, notably the marine coccolithophorids *Emiliania huxleyi* and *Gephyrocapsa oceanica* [e.g., *Volkman et al.*, 1980; *Marlowe et al.*, 1984; *Conte et al.*, 1992], and presumably other living and extinct members of the family *Gephyrocapsae* [*Marlowe et al.*, 1990; *Müller et al.*, 1998], have or have had the capability to synthesize alkenones whose extent of unsaturation changes with growth temperature [*Marlowe et al.*, 1984; *Brassell et al.*, 1986; *Prahl and Wakeham*, 1987]. On the basis of this correlation, paleo-SST can be calculated from the so-called ketone unsaturation index U^{K}_{37} [e.g., *Brassell et al.*, 1986; *Prahl and Wakeham*, 1987; *Müller et al.*, 1998]. Here, we used the simplified version of the index $U^{K}_{37}{}'$ [*Prahl and Wakeham*, 1987; *Müller et al.*, 1998]:

$$U^{K}_{37}{}' = [C_{37:2}]/[C_{37:2} + C_{37:3}] \text{ or } SST = \left[U^{K}_{37}{}' - 0.044\right]/0.033$$

because of the generally low abundance of $C_{37:4}$ alkenones and for consistency to existing records from the North Atlantic [e.g., *Rosell-Melé et al.*, 1997; *Villanueva et al.*, 1997, 2001; *Bard et al.*, 2000; *Calvo et al.*, 2001; *Rosell-Melé*, 2001]. Following these authors, we assume that the alkenone-based SSTs mainly display in situ SST and a major influence of reworked alkenones can be neglected. In the few intervals with increased abundance of $C_{37:4}$ alkenones reaching about 3–7.5% of total C_{37} alkenones and coinciding with minimum SST, SST minima of the U1313 record would become even lower when using the U^{K}_{37} calibration [cf. *Bard et al.*, 2000]. A $C_{37:4}$ concentration of 1% and 7.5%, for example, would result in an additional temperature decrease of 0.4°C and 3.3°C, respectively.

[14] Salinity perturbations in the northern North Atlantic as expected for periods of massive ice and iceberg melting, e.g., during Heinrich-type IRD events, may also be reflected

[1] Auxiliary materials are available at http://dx.doi.org/10.1594/PANGAEA.712917.

in the occurrence and relative abundance of the C_{37} tetraunsaturated alkenone ($C_{37:4}$), as shown in studies of several North Atlantic sediment cores [e.g., *Rosell-Melé*, 1998; *Bard et al.*, 2000; *Rosell-Melé et al.*, 2002; *Sicre et al.*, 2002; *Martrat et al.*, 2007]. This approach, i.e., the relative abundance of $C_{37:4}$, has been used as first-order proxy for the identification of meltwater influence in the U1313 record.

[15] For the high-resolution biomarker study carried out on 240 samples from the interval of 14–21 mcd (about 320–460 ka) a time resolution of about 580 years was obtained.

[16] In addition to the analyses done at AWI on primary splice samples, further data were produced at the laboratory of the Departamento de Geologia Marinha of LNEG and at MARUM/Bremen University on a different set of samples from the secondary splice, representing the time interval of about 340–640 ka. The >315 μm fraction was used to pick foraminifers for stable isotope analysis and for counting lithic fragments. Lithic abundance is presented as "number of grains per gram sediment" and primarily interpreted as IRD. Here, we are aware that the >315 μm fraction probably only picks up the major IRD events whereas the more commonly used >150μm is more reliable for baseline changes in IRD [cf. *McManus et al.*, 1999]. Using such a relative coarse size fraction for IRD in the U1313 sequence, we are able to detect all the major IRD events as evidenced from the good correlation between IRD and XRD records. Benthic δ^{18}O values were measured on 2–4 specimens of *Cibicidoides wuellerstorfi* or in a few levels *Uvigerina* sp. in a Finnigan MAT 252 mass spectrometer at MARUM/Bremen University; all *Cibicidoides* values were then corrected by adding +0.64‰ [*Shackleton*, 1974]. In this paper, we mainly use the benthic δ^{18}O record for age model development. In the major trends, the Site U1313 record replicates the DSDP Site 607 data (Figure 2), but absolute values differ (see comment by M. Raymo on http://www.maureenraymo.com/climate_archives.php for potential reason). Because of its higher resolution, the Site U1313 series shows more pronounced substages and higher-frequency oscillations within MIS 12 and 15. For further interpretation of the stable isotope data as well as more details on methods we refer to A. Voelker et al. (High-frequency changes in surface and deep water hydrography in the mid-latitude North Atlantic during marine isotope stages 11–15: New insights from IODP Sites U1313 and U1308, unpublished manuscript, 2008).

3. Age Model and Accumulation Rates

[17] In this study we use the LR04 time scale based on a stack of 57 globally distributed benthic oxygen isotope (δ^{18}O) records [*Lisiecki and Raymo*, 2005] as a stratigraphic reference. The benthic δ^{18}O record of Site 607 that was originally published by *Raymo et al.* [1989], *Ruddiman et al.* [1989], and *Raymo* [1992] is part of the LR04 stack. Thus, a very detailed correlation of physical (e.g., lightness L*) and chemical (e.g., $CaCO_3$, benthic isotopes) sediment properties measured at Sites U1313 and 607 enabled us to develop an age model for the studied time interval from 320 to 640 ka of Site U1313 that is directly comparable to the LR04 stack (Figure 2). The age model is supported by the new high-resolution benthic oxygen isotope record (Figure 2) measured on the secondary splice (Holes A and D) of Site U1313 and directly tuned to the LR04 stack (Voelker et al., unpublished manuscript, 2008). For our study we adopted this isotope stratigraphy by converting the depth scale of the secondary splice into the depth scale of the primary splice (Holes B and C) through a correlation of the L* records of both splices (Figure 2). Potential sources of error in the Site U1313 age model are mismatches resulting from the tuning process (which we tried to minimize) and uncertainty in the chronology of the benthic isotope stack itself which is estimated to be ~4 ka in the time interval 1–0 Ma [*Lisiecki and Raymo*, 2005].

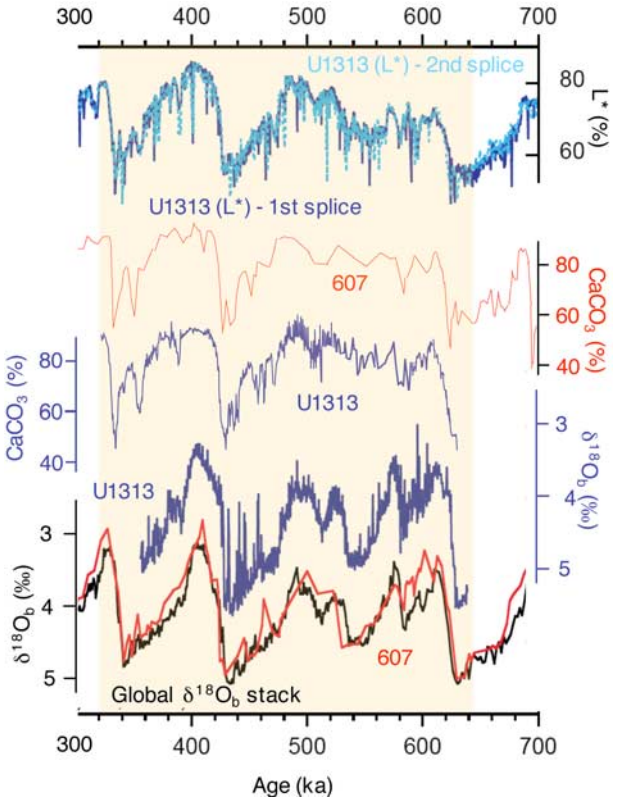

Figure 2. Parameters used for constructing the age model at Site U1313: lightness (L*) from color reflectance measurements of the first and second splices [*Expedition Scientists*, 2005]; $CaCO_3$ determined at Site U1313 in comparison to the $CaCO_3$ record from Site 607 [*Ruddiman et al.*, 1989]; high-resolution benthic isotope (δ^{18}O) record from Site U1313 (second splice; details in the work by Voelker et al. (unpublished manuscript, 2008)) in comparison to the benthic LR04 δ^{18}O stack of *Lisiecki and Raymo* [2005] and the benthic δ^{18}O curve for Site 607 [*Raymo et al.*, 1989; *Ruddiman et al.*, 1989; *Raymo*, 1992].

[18] Using linear sedimentation rates (LSR in cm ka^{-1}) based on this age model and dry bulk density (DBD in g cm^{-3}),

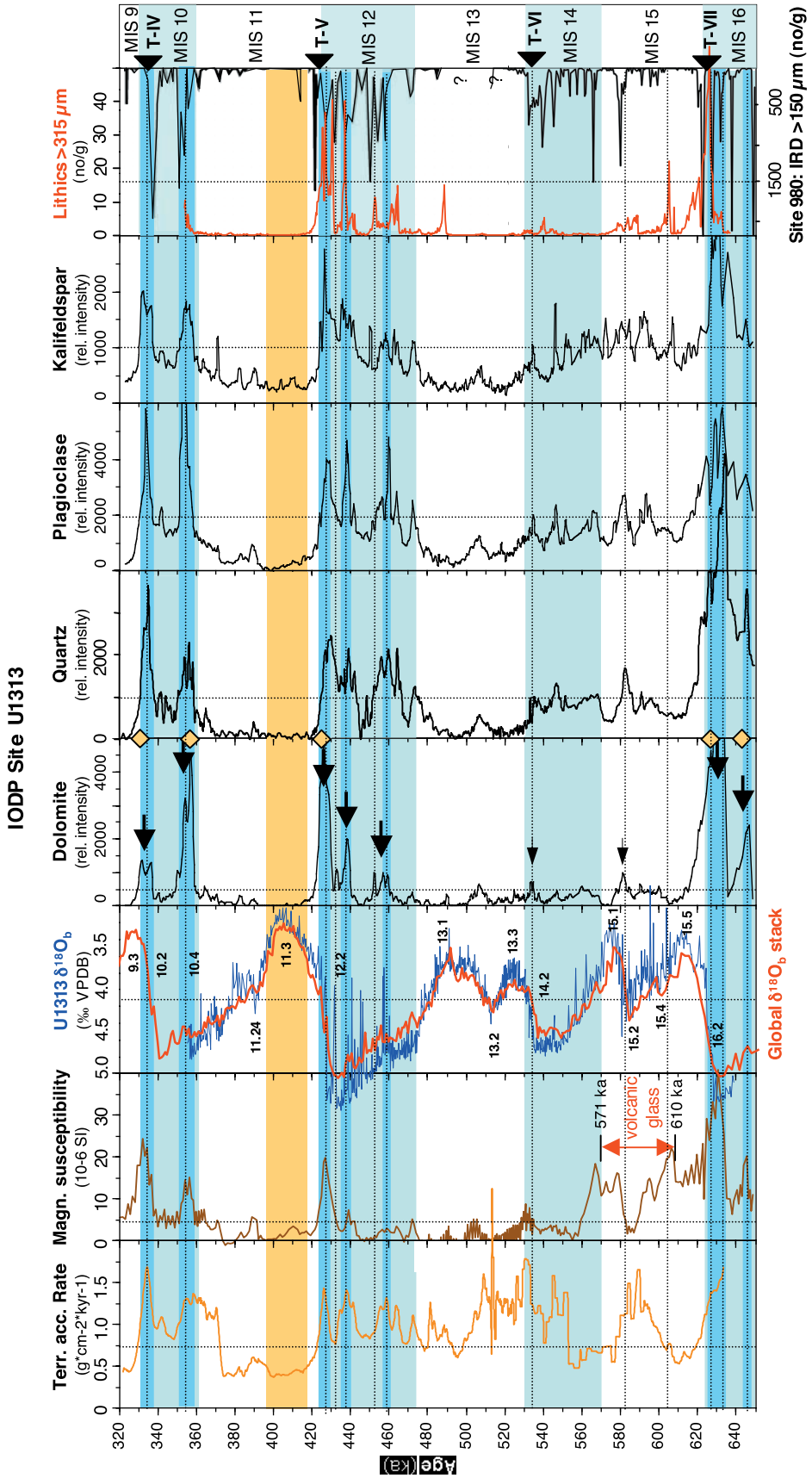
IODP Site U1313
MIS 9
T-IV
MIS 10
MIS 11
T-V
MIS 12
MIS 13
T-VI
MIS 14
MIS 15
T-VII
MIS 16
Lithics >315 µm (no/g)
Site 980: IRD >150 µm (no/g)
Kalifeldspar (rel. intensity)
Plagioclase (rel. intensity)
Quartz (rel. intensity)
Dolomite (rel. intensity)
U1313 δ18Ob (‰ VPDB)
Global δ18Ob stack
Magn. susceptibility (10-6 SI)
571 ka
volcanic glass
610 ka
Terr. acc. Rate (g*cm-2*kyr-1)
Age (ka)

Figure 3

accumulation rates (AR in g cm^{-2} ka^{-1}) of total sediment (TS) were calculated [see *van Andel et al.*, 1975]:

$$TS\_AR = LSR * DBD.$$

DBD was obtained from gamma ray attenuation (GRA) wet bulk density (WBD) measurements using the equation DBD = −1.6047 + 1.5805 * WBD. The linear relationship between wet bulk density and dry bulk density measurements is derived from shipboard moisture and density measurements performed on discrete samples [*Expedition Scientists*, 2005].

[19] Using carbonate ($CaCO_3$ in %) and total organic carbon (TOC in %) values and assuming that biogenic silica can be neglected [see *Expedition Scientists*, 2005], accumulation rates of nonbiogenic (terrigenous) sediment were calculated as

$$Terr\_AR = TS\_AR *(100 - CaCO_3 - TOC)/100.$$

4. Results

4.1. Downcore Variability in IRD Proxies

[20] For MIS 16–9, relative XRD intensities of quartz (4.26 Å), plagioclase (3.19 Å) and kalifeldspar (3.24 Å) and dolomite (2.89 Å) were determined to be used as proxy for detrital input from surrounding continents. In general, all these detrital minerals show distinct peak values during glacial stages MIS 16, 12, and 10, whereas minimum values occur in MIS 13, 11, and 9 (Figure 3). Most of the peak values (i.e., MIS 16, upper MIS 12, and MIS 10) also coincide with maximum magnetic susceptibility values (Figure 3). During MIS 15 and 14, relative intensities of quartz, plagioclase, and kalifeldspar are higher than those determined for MIS 13, 11, and 9, but significantly lower than the peak values of MIS 16, 12, and 10. In contrast to the other interglacials, MIS 15 is characterized by quite high feldspar values. Furthermore, within the studied time interval MIS 15 is also unique because of its high abundances of tephra grains; that is, lithics in this interval consist either exclusively or to large amounts of fresh volcanic glass including large pumice pieces (Voelker et al., unpublished manuscript, 2008). Thus, the XRD signal cannot be interpreted as IRD during MIS 15.

4.2. Downcore Variability in Biomarkers: Organic Carbon Composition and Sea Surface Temperature

[21] For the interpretation of the TOC record in terms of paleoenvironment, information on the composition of the organic matter is needed. On the basis of high-resolution biomarker records available for MIS 12–9, a distinct variability between input of terrigenous organic matter (indicated by the long-chain *n*-alkanes) and marine organic matter related to phytoplankton productivity (indicated by the long-chain alkenones), is obvious (Figure 4). Both, input of terrigenous organic matter as well as phytoplankton productivity, seem to be increased during the glacials and decreased during the interglacials. Both records, however, show differences when looking into details. Whereas the long-chain *n*-alkanes show distinct maxima at the MIS 11/12 and 9/10 transitions (i.e., near terminations V and IV) and the lower part of the glacials, the maxima in alkenones occur in the middle part of the glacials MIS 12 and 10, generally coinciding with TOC maxima (Figure 4).

[22] Alkenone-based sea surface temperatures (SST) determined for MIS 12–9, show a strong variability between 8 and 19°C (Figure 4). Maximum SST of 19°C and 18°C were measured in the peak interglacial sections of MIS 11 and MIS 9, respectively. Furthermore, significant cooling events of 3–4°C were found in MIS 11. Minimum SST values of 8–10°C occur in MIS 12 and 10. Terminations V and IV are characterized by sharp SST increases from 8 to 18°C and 9 to 18°C, respectively. In general, there is a good correlation between SST and carbonate content. Carbonate contents >80% and SSTs > 14°C are dominant during interglacials MIS 11 and 9, whereas during glacials MIS 12 and 10 carbonate contents are <80% and SSTs < 15°C are typical.

5. Discussion

5.1. Heinrich-Like Events and Ice Sheet Instability

[23] On the basis of numerous sedimentological and geochemical studies, amount and composition of detrital coarse fraction in sediment cores from the North Atlantic give information about the input of ice-rafted debris (IRD) [e.g., *Bond et al.*, 1992; *Andrews and Tedesco*, 1992; *Gwiazda et al.*, 1996; *van Kreveld et al.*, 1996; *Moros et al.*, 2002, 2004]. Here, especially the enrichment of dolomite in sedimentary sections is indicative for IRD input

Figure 3. Accumulation rates of terrigenous sediment fraction; magnetic susceptibility (determined by GEOTEK multisensor core logging [*Expedition Scientists*, 2005]); three-point-moving averages of relative XRD intensities of dolomite, quartz (4.26 Å), plagioclase, and kalifeldspar; and lithic grains >315 μm (number per gram sediment), determined in samples from IODP Site U1313 and plotted versus age (320–650 ka). Between 571 and 610 ka, the occurrence of volcanic glass is indicated (Voelker et al., unpublished manuscript, 2008). In addition, the global benthic isotope stack of *Lisiecki and Raymo* [2005] and high-resolution benthic isotope ($\delta^{18}O$) record from Site U1313 (second splice; details in the work by Voelker et al. (unpublished manuscript, 2008)) are shown. Furthermore, at the right-hand side of the plot an IRD record of ODP Site 980 is shown. The time interval of 320 to about 500 ka is from *McManus et al.* [1999], and the time interval of about 513–650 ka is from *Wright and Flower* [2002]; question marks show data gap between both records. Most prominent Heinrich-like events in MIS 10, 12, and 16 are marked by large black arrows; two minor (Heinrich-like?) events at the MIS 15.2/15.1 transition and at Termination VI are marked by small black arrows. Orange rhombs indicate occurrence of Heinrich-like events at IODP Site U1308 [*Hodell et al.*, 2008]. Marine isotope stages (MIS) 9–16 and terminations IV, V, VI, and VII are indicated; orange bar highlights peak interglacial MIS 11.3.

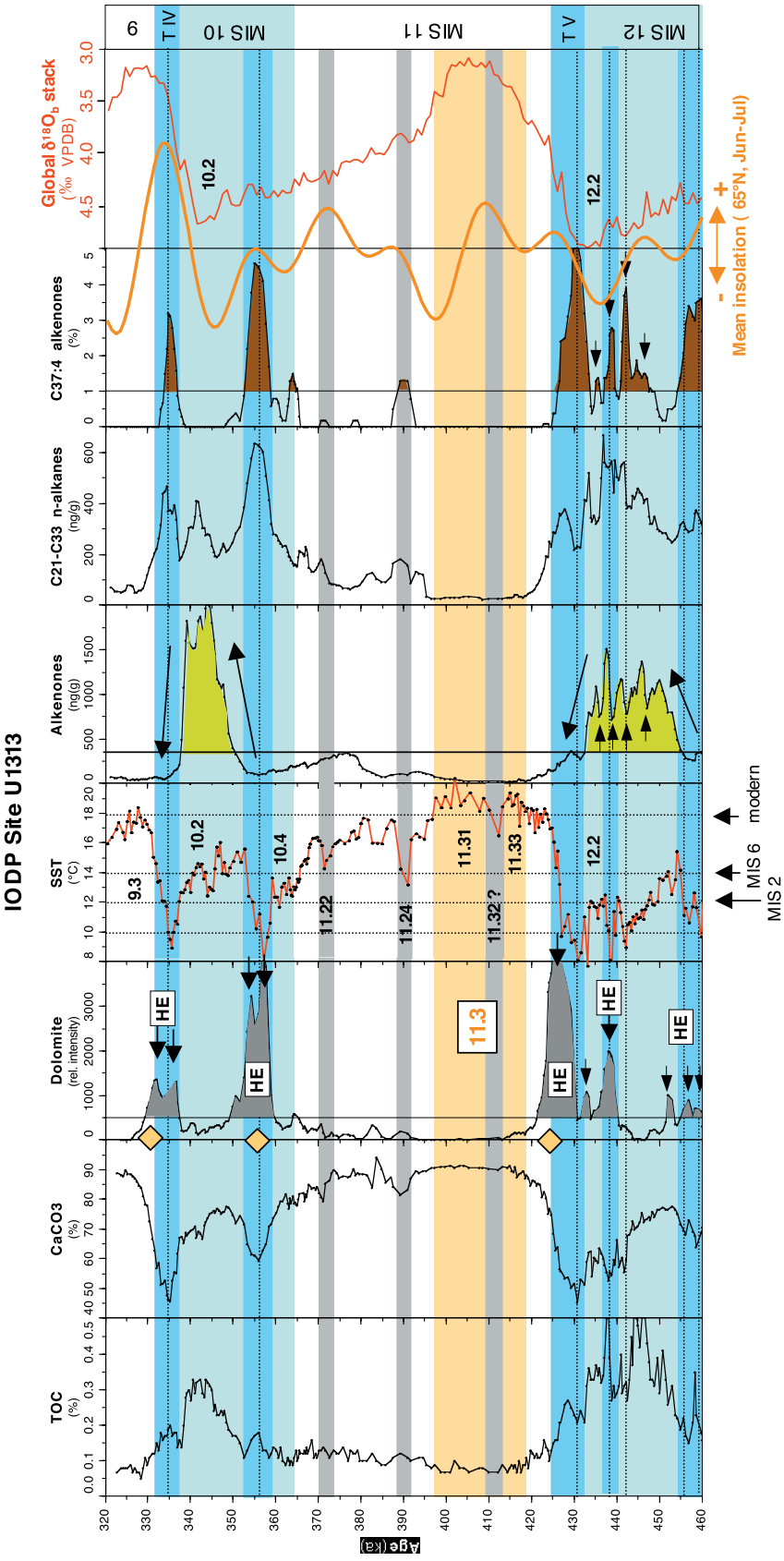

Figure 4. High-resolution records of three-point-moving averages of TOC, $CaCO_3$, relative XRD intensities of dolomite, absolute abundance of alkenones and long-chain *n*-alkanes (ng g^{-1}), relative abundance of $C_{37:4}$ alkenones (in percent of sum of C_{37} alkenones), and alkenone-based sea surface temperatures (SST). In addition, the global benthic isotope stack of *Lisiecki and Raymo* [2005] and mean summer insolation at 65°N [*Laskar et al.*, 2004] are shown. Orange rhombs indicate occurrence of Heinrich-like events at IODP Site U1308 [*Hodell et al.*, 2008] (see Figure 1 for location). Marine isotope stages and substages (according to *Bassinot et al.* [1994]), terminations IV and V, and Heinrich-like events (HE) are indicated; orange bar highlights peak interglacial MIS 11.3. Vertical arrows at the bottom of the SST graph indicate modern SST [*Locarnini et al.*, 2006] and SST of MIS 6 and MIS 2 (compare Table 1).

from a quite restricted area around Hudson Strait, whereas detrital quartz and feldspars are probably more general proxies for continental-derived material. As outlined by *Moros et al.* [2004], for example, ice rafting of quartz grains has recently been particularly effective in the shelf areas close to Greenland and Labrador, and more extensive ice rafting during the last glaciation caused high quartz abundances to occur in the central areas of the North Atlantic [*Biscaye*, 1965; *Kolla et al.*, 1979; *Leinen et al.*, 1986]. Occurrence and variability of input of these coarse-grained detrital fractions can be related to instabilities of the surrounding ice sheets. Most of the studies on Heinrich events are restricted to the last glacial/interglacial cycle (MIS 5 to MIS 1), whereas high-resolution studies dealing with sub-Milankovitch variabilities of IRD input into mid-latitude North Atlantic and going back in time of several 100,000 years are still more limited [e.g., *Oppo et al.*, 1998; *McManus et al.*, 1999; *Wright and Flower*, 2002; *Bauch and Erlenkeuser*, 2003; *de Abreu et al.*, 2003].

[24] In a 0.5 million years record from ODP Site 980 (see Figure 1 for location), *McManus et al.* [1999] recognized a relationship between benthic $\delta^{18}O$ and both the initial and final IRD pulses for each 100-ka cycle. That means, an IRD event follows the first increase in benthic $\delta^{18}O$ after exceeding a threshold value, and a second prominent IRD event occurred during rapid deglaciations [*Broecker and van Donk*, 1970; *McManus et al.*, 1999]. On the basis of this obvious close association of the onset and cessation of ice-rafting events with a particular value in the benthic $\delta^{18}O$ proxy for ice volume, *McManus et al.* [1999] proposed that this value represents an important threshold in ice sheet growth. Our new data support this hypothesis. Two distinct peaks in IRD occurred in all the three major glacials MIS 16, 12 and 10, i.e., near the beginning and end of the glacials (Figure 3). For these time intervals, pulses of IRD at Site U1313 seem to be almost contemporaneous to similar pulses recorded at Site 980 (Figure 3) [*McManus et al.*, 1999; *Wright and Flower*, 2002], suggesting widespread IRD discharge within as well as north of the IRD belt. These main IRD events with a duration of a few thousand years are reflected in prominent peaks in dolomite, quartz, and feldspars, and magnetic susceptibility (Figure 3). During the most severe glacial MIS 12, even three additional smaller dolomite peaks were determined. Furthermore, the IRD peaks in MIS 16, 12, and 10 coincide with increased accumulation rates of terrigenous matter (Figure 3), confirming that these peaks are related to enhanced IRD input [cf. *McManus et al.*, 1998].

[25] On the basis of these characteristics, the most prominent IRD pulses in MIS 16, 12, and 10 are classified as Heinrich-like events. Major source of the IRD is the Hudson Strait area as indicated by the dolomite peaks. A Hudson Strait source is also supported by specific biomarker associations found in the Heinrich-like layers at Site U1313 [*Hefter et al.*, 2007; cf. *Rashid and Grosjean*, 2006]. Reinvestigation of available geologic and organic geochemical data even allowed narrowing down this assumed source to an Ordovician oil shale close to Hudson Strait, that indeed bears a striking resemblance in terms of biomarker distributions when compared to the specific association of compounds from samples of Heinrich-type events [*Hefter et al.*, 2007]. Contemporaneously with these events determined at Site U1313, distinct Ca/Sr maxima were identified in Site U1308 located in the central part of the IRD belt, also interpreted as Heinrich-like events [*Hodell et al.*, 2008]. These events indicate a major instability of the Laurentide Ice Sheet and discharge of icebergs during the early and late (to deglacial) phase of major glaciations [cf. *Broecker and van Donk*, 1970; *McManus et al.*, 1999].

[26] During the weaker glacial MIS 14 characterized by smaller ice volume, IRD concentrations were much lower than during MIS 16 and 12, as indicated by low dolomite abundances and an almost absence of lithic grains >315 μm (Figure 3). Thus, the increased accumulation rates of (fine-grained) terrigenous matter in the upper part of MIS 14 (Figure 3) have to be explained by other processes such as, for example, increased current-controlled input of fine fraction rather than IRD input. Further more detailed work on grain size distribution of the silt fraction as well as on clay mineralogy, however, are needed to prove this hypothesis. In the area north of the IRD belt, on the other hand, significant IRD input also continued during MIS 14, as reflected in the elevated IRD numbers at Site 980, suggesting the close-by British Islands as possible source region (Figure 3) [*McManus et al.*, 1999; *Wright and Flower*, 2002].

[27] In general, IRD is diminished during interglacials MIS 13, MIS 11, and MIS 9.3. In interglacial MIS 15, on the other hand, some intervals with increased feldspar and magnetic susceptibility values are obvious, related to the presence of coarse-grained volcanic glass particles (Figure 3). According to Voelker et al. (unpublished manuscript, 2008), the tephra grains look fresh throughout the whole interval and seem to be from an aerial eruption, suggesting the Azores island volcanoes as possible source area rather than ice-rafted tephra from Iceland. Increased input of volcanic glass may also explain the elevated accumulation rates of terrigenous matter at that time (Figure 3). A small IRD peak (i.e., maxima in dolomite, quartz, and feldspars) occurred at the MIS 15.2/15.1 transition, coinciding with an IRD peak at ODP Site 980 (Figure 3), which may reflect a (minor) Heinrich-like event at that time.

[28] MIS 11.3 is the most extreme interglacial with no coarse-grained IRD > 315 μm, no dolomite, insignificant amount of quartz, minimum magnetic susceptibility values, and minimum accumulation rates of terrigenous matter (Figure 3). The absence of major continental ice at the coastal North Atlantic as well as too warm sea surface temperatures preventing IRD transport toward the site location (see section 5.2 for further discussion), may explain the lack of IRD at Site U1313. Long-lasting, ice-free conditions in the North Atlantic during interglacial MIS 11.3 were also described in other North Atlantic sediment cores further to the north such as, for example, ODP Site 980 and Core PS1243 [*McManus et al.*, 1999; *Bauch and Erlenkeuser*, 2003] (see Figure 1 for core location). This may support that the absence of major amounts of IRD is most likely related to the simple requirement of sufficient continental ice near the North Atlantic prior to catastrophic

discharge, a prerequisite not fulfilled during peak interglacials [*McManus et al.*, 1999].

[29] Additional to the most prominent IRD (Heinrich-like) events indicated by the dolomite peaks, further detrital peaks are visible in the quartz and feldspar records (Figure 3). There seem to be millennial-scale oscillations in relative abundances of these minerals during the most prominent glacials MIS 12 and 10, but even during MIS 15 and 14. This millennial-scale variability is most obvious in the plagioclase and kalifeldspar records. The different mineralogical signature may point to a different source of the detrital fraction such as Greenland, Labrador or Scandinavia. At IODP Site U1308, millennial-scale peaks in the Si/Sr record interpreted as proxy for input of detrital silicate minerals, also occur much more frequently than Heinrich-like events and may represent a different source [*Hodell et al.*, 2008]. Future Pb isotopes to be measured in single feldspar grains from these IODP cores [e.g., *Gwiazda et al.*, 1996] as well as K-Ar and $^{87}Sr/^{86}Sr$ isotope studies [*Huon and Ruch*, 1992] may help to identify source areas more precisely.

5.2. Variability of Sea Surface Temperature in the Midlatitude North Atlantic

[30] Before discussing and interpreting the new SST data from Site U1313, let us start with a short discussion of SST characteristics in the midlatitude North Atlantic during the younger glacial/interglacial cycles, especially during MIS 6 and MIS 2. On the basis of planktonic foraminifer assemblages and modern analog technique, reconstruction of the Last Glacial Maximum (LGM) summer and winter SST in the North Atlantic indicates that the Polar Front was situated at about 42–46°N during that time, extending in an east–west direction and resulting in a steep south–north SST gradient (Figure 1) [*Pflaumann et al.*, 2003; *Sarnthein et al.*, 2003]. Across the LGM Polar Front, alkenone SST estimates were determined in two sediment cores from areas south of (MD952037) and within (SU90-08) the Polar Front [*Calvo et al.*, 2001]. In both cores, SST variations show a clear glacial/interglacial evolution and provide evidence for changes in paleoceanographic conditions during the last about 300 ka. However, both records also display very different values for specific glacials, indicating varying climatic conditions (e.g., the location of the Polar Front) in these glacial periods [*Calvo et al.*, 2001; *de Abreu et al.*, 2003]. Whereas the southern Core MD952037 recorded similar SST values during the MIS 2 and MIS 6 glacial periods (ca. 14–15°C), the northern Core SU90/08 displayed colder conditions during MIS 2/LGM (8–10°C) than in MIS 6 (13–15°C) (Table 1). According to *Calvo et al.* [2001], these results indicate the existence of a well-developed steep north–south gradient of about 6°C between 37 and 43°N during the LGM but not during MIS 6, which suggests a southern expansion of the polar waters during the LGM. Alkenone-based SST values determined in samples from Site U1313 across Termination I (MIS2/1) and Termination II (MIS 6/5) fit very well in between the two SST records from the cores south (MD952037) and north (SU90-08) of Site U1313 (Table 1), supporting the differences in SST gradients during MIS 6 and MIS 2, proposed by *Calvo et al.* [2001].

[31] Our new high-resolution SST record of the time interval 460–320 ka at IODP Site U1313 indicate a distinct glacial/interglacial as well as sub-Milankovitch variability. Maximum SST values of 19°C were reached during MIS 11.3, values which are similar to those of MIS 5.5 and about 1–2°C warmer than those of today and MIS 9.3 (Figure 4). During IRD events of glacial stages MIS 12 and 10, minimum SST values of about 8°C were determined at Site U1313. This variability in SST correlates well with the variability in SST based on planktonic foraminifers from Site 607 [*Ruddiman et al.*, 1989].

[32] Looking at the SST record of Site U1313 in more detail, it is obvious that peak warmth of about 19°C was reached during MIS 11.3 (397–418 ka), interrupted by a short cooling event of 1–2°C around 413 ka (Figure 4). Maximum SST already occurred prior to the global benthic isotope ($\delta^{18}O$) minimum (sea level highstand) and thus prior to peak interglacial conditions (see also benthic $\delta^{18}O$ record of Site U1313 (Figure 4)). In the upper half of MIS 11, SSTs continuously decreased (contemporaneously with increasing $\delta^{18}O_b$ values), with two cooling events around 390 and 372 ka (MIS 11.24 and 11.22), for which glacial (MIS 6 and MIS 10.2) temperatures of 13–14°C were determined (see Table 1). While MIS 11.3 SSTs are similar to those recorded off southwestern Portugal [*Martrat et al.*, 2007], Site U1313 experienced less temperature oscillations during the glacial inception, probably because of a fairly persistent influence of the Gulf Stream/North Atlantic Drift which inhibited subpolar waters to be advected to Site U1313.

[33] During glacials MIS 12 and 10, SSTs show a high-amplitude variability of about 4–7°C which is significantly higher than those of interglacials. Interestingly to note, absolute minimum SSTs did not occur during peak glacials. During MIS 10.2, SST reached 13–15°C, i.e., values similar to those of MIS 6. During MIS 12.2, the most severe glaciation of the last 0.5 Ma [*Shackleton*, 1987], SSTs of about 11–12°C were determined, i.e., values similar to those of MIS 2. The absolute SST minima, on the other hand, occurred directly before the glacial maximum as well as at the end, i.e., during the termination (Figure 4). This is most distinctly obvious for MIS 10.2. These SST minima are correlated to Heinrich-like events and related meltwater pulses, most prominent during terminations V and IV. Across terminations V and IV, i.e., around 427 ka and 365 ka, SST increase was very abrupt and prominent reaching about 10°C and 9°C, respectively (Table 1).

[34] In terms of variability as well as absolute values, the SST record of Site U1313 within MIS 11 to MIS 9 is quite similar to the alkenone-based SST record of Core MD012443 taken from the Iberian continental margin at a similar latitude as Site U1313 (37°52.85′N, 10°10.57′W; see Figure 1 for location). At that Site, SST reached maximum values of about 19°C during MIS 11, followed by a SST decrease with single minima as low as about 8°C during MIS 10 and a rapid warming of about 11°C during the MIS 10/9 transition (Termination IV) [*Martrat et al.*, 2007]. This suggest that prominent cold water pulses may have reached the Iberian margin during MIS 10, pulses which may be explained by meltwater events similar to those observed

Table 1. Mean Alkenone-Based Surface Water Temperatures for Specific Glacial and Interglacial Intervals and Heinrich-Like Events and SST Changes Across Terminations I, II, IV, and V[a]

	Core		
	MD952037	U1313	SU90-08
Latitude	37°N	40°N	43°N
MIS 1	19	18	17
MIS 2	15	12	9
Termination I	4	6	8
MIS 5	21	19	19
MIS 6	14	14	14
Termination II	7	5	5
MIS 9	N.D.	18	N.D.
MIS 10 (final HE)	N.D.	9	N.D.
MIS 10.2	N.D.	13	N.D.
Termination IV	N.D.	9	N.D.
MIS 11	N.D.	18	N.D.
MIS 12 (final HE)	N.D.	8	N.D.
MIS 12.2	N.D.	12	N.D.
Termination V	N.D.	10	N.D.

[a]Temperatures are in °C. Data from cores MD952037 and SU90-08 are from *Calvo et al.* [2001]; data from Site U1313 are our own data. N.D., no data. Across terminations IV and V, the extreme increase in SST is caused by meltwater pulses related to Heinrich-like events (HE) at the end of MIS 12.2 and MIS 10.2.

during Heinrich events 1–3 [*Bard et al.*, 2000] (see section 5.3 for more details).

5.3. Heinrich-Like Events and Surface Water Characteristics

[35] In several studies of sediment cores from the North Atlantic representing (part of) the last climatic cycle, biomarker proxies were used to get information about surface water characteristics, ice sheet instability, and related Heinrich events [e.g., *Rosell-Melé et al.*, 1997, 2002; *Villanueva et al.*, 1997; *Rosell-Melé*, 1998, 2001; *Bard et al.*, 2000; *Calvo et al.*, 2001]. On the basis of these studies, for example, changes in alkenone-derived SST show that the ocean surface water underwent significant cooling during periods of Heinrich events, probably as a result of incoming meltwater. Increased meltwater influx is reflected in elevated abundance of the $C_{37:4}$ alkenone concentration linked to a reduction of surface water salinity. With the new data on amount and composition of IRD and alkenone data from IODP Site U1313 we were able to extent this type of climate record further back in time.

[36] As obvious from the records in Figure 4, there seems to be a general relationship between IRD (dolomite) peaks, SST, and amount and composition of the organic carbon fraction, manifested in the record as Heinrich-like events similar to those described for the last climate cycle. The coincidence of dolomite maxima, absolute SST minima and peaks in $C_{37:4}$ alkenones indicate that a sudden instability of the Laurentide Ice Sheet causing huge input of IRD and pulses of cold, low-saline meltwater, have controlled the surface water characteristics in the midlatitude central North Atlantic. Within the cold meltwater, icebergs could survive the long-distance transport into the central Atlantic. The ice-rafted material was also enriched in terrigenous organic carbon, as indicated by maxima in long-chain *n*-alkane abundance (Figure 4). At the most prominent meltwater event during Termination V, it is interesting to note that SST minimum and $C_{37:4}$ maximum, indicating the presence of cold, low-saline water, are preceding the main IRD (dolomite) peak. That means, an already existing meltwater lid may have helped IRD to reach the study site at that time.

[37] On the basis of our age model, SST minima correlate with insolation maxima, and the same correlation to insolation maxima is obvious for the major Heinrich-like events during MIS 12 and 10 (Figure 4). This may indicate that the ice sheet instability/melting and subsequent discharge of icebergs and meltwater was triggered by increased insolation in the high latitudes. During glacial maxima MIS 10.2 and 12.2 coinciding with insolation minima, on the other hand, the huge ice sheets were more stable, preventing IRD input into the North Atlantic. Even during the cold phase MIS 11.24 when SSTs decreased to values similar to MIS 6 (Figure 4), inflow of polar waters probably occurred. The input of detrital matter, however, was of secondary significance, although minor maxima in magnetic susceptibility, quartz, feldspars, and accumulation rates of terrigenous matter (Figure 3) as well as minor maxima in terrigenous organic matter and $C_{37:4}$ alkenones are obvious (Figure 4).

[38] TOC values display distinct maxima during glacials MIS 12 and MIS 10 whereas during interglacial MIS 11 TOC values are <0.1%. The TOC maxima coincide with maxima in absolute abundance of alkenones (indicative for coccolithophorides), whereas alkenones are almost absent during MIS 11 (Figure 4). Thus, it seems to be that during glacial maxima (excluding periods of Heinrich-like events), surface water productivity in the central midlatitude North Atlantic was generally increased, probably because of a more southern position of the Polar Front [*Villanueva et al.*, 2001]. Together with the Polar Front nutrient-enriched subpolar central water could advance southward, which would allow nutrients to be replenished during deep winter mixing. In addition, increased dust (and nutrient) supply from the Sahara as recorded for the LGM interval [e.g., *Sarnthein et al.*, 1981], may have triggered increased surface water productivity during MIS 12 and 10. Higher glacial nutrient levels in surface waters are also indicated by the planktonic $\delta^{13}C$ values (Voelker et al., unpublished manuscript, 2008).

[39] The increase in phytoplankton productivity started after the initial Heinrich-like event, and productivity decreased with the onset of the final Heinrich-like event during the termination (Figure 4). During Heinrich-like events, the strongly increased discharge of meltwater and release of suspended matter from melting icebergs during terminations V and IV have probably resulted in unfavorable conditions for phytoplankton productivity [cf. *van Kreveld et al.*, 1996; *Nave et al.*, 2007], i.e., in a more or less complete collapse of phytoplankton productivity, as indicated by the abrupt drop in alkenone abundance to almost zero.

[40] Within the interval of generally enhanced phytoplankton productivity during MIS 12, millennial-scale oscillation in productivity is obvious. Between about 452 and 435 ka, at least four minima in absolute alkenone abundance, i.e., episodes of reduced productivity, occurred,

coinciding with $C_{37:4}$ peaks indicative for meltwater discharge (Figure 4).

6. Conclusions

[41] Records of quartz, feldspars, dolomite, carbonate, magnetic susceptibility, amount and composition of organic carbon, alkenone-based sea surface temperature (SST), and accumulation rates of terrigenous matter determined at IODP Site U1313 for Marine Isotope Stage (MIS) 9–16 allow the following main conclusions.

[42] 1. Most prominent IRD events characterized by peaks in dolomite, quartz, feldspars, and magnetic susceptibility as well as increased accumulation rates of terrigenous matter, are interpreted as Heinrich-like events, documenting episodes of enhanced iceberg delivery into the central midlatitude North Atlantic due to sudden instability of the Laurentide Ice Sheet. These major events occurred during the early and late (deglacial) phases of glacials MIS 16, 12, and 10.

[43] 2. During the time interval MIS 12–9, alkenone-based SST shows a strong variability between 8 and 19°C. Maximum SST of about 19°C was reached during MIS 11.3 (397–418 ka). In the upper half of MIS 11, two cooling events occurred around 390 (MIS 11.24) and 372 ka (MIS 11.22), for which almost glacial (MIS 6 and MIS 10.2) temperatures of 13–14°C were determined. Absolute SST minima of 8–10°C are correlated to meltwater pulses and related Heinrich-like events, most prominent near the onset and the late (termination) phase of glacials MIS 12 and 10. Across terminations V (~427 ka) and IV (~365 ka) SST increase was very abrupt and distinct reaching 9–10°C. During Termination V, the very strong meltwater signal seems to precede the IRD signal.

[44] 3. On the basis of our age model, SST minima and major Heinrich-like events during MIS 12 and 10 correlate with insolation maxima. This may indicate that the ice sheet instability/melting and subsequent discharge of icebergs and meltwater was triggered by increased insolation in the high northern latitudes. During glacial maxima MIS 12.2 and 10.2 coinciding with insolation minima, on the other hand, the huge ice sheets were more stable, preventing IRD input into the North Atlantic.

[45] 4. TOC maxima coinciding with maxima in absolute abundance of alkenones, occurred during MIS 12 and 10 and are interpreted as periods of increased surface water productivity in the central midlatitude North Atlantic during glacial maxima (excluding periods of Heinrich-like events) due to a closer position of the Polar Front to the coring site. During Heinrich-like events, huge input of meltwater and release of suspended matter from melting icebergs during terminations IV and V have probably caused a more or less complete collapse of phytoplankton productivity, as indicated by the abrupt drop in alkenone abundance to almost zero.

[46] **Acknowledgments.** This research used samples and data provided by the Integrated Ocean Drilling Program. For technical support, we thank Walter Luttmer. We also thank the four anonymous reviewers for numerous constructive suggestions for improvement of the manuscript. Funding by the German Research Foundation (grant STE 412/23-1) and the Portuguese Foundation for Science and Technology (grants PDCT/MAR/58282/2004 and SFRH/BPD/21691/2005) are gratefully acknowledged.

References

Andrews, J. T., and K. Tedesco (1992), Detrital carbonate-rich sediments, northwestern Labrador Sea: Implications for ice-sheet dynamics and iceberg rafting (Heinrich) events in the North Atlantic, *Geology*, *20*, 1087–1090, doi:10.1130/0091-7613(1992)020<1087:DCRSNL>2.3.CO;2.

Andrews, J. T., K. Tedesco, and A. E. Jennings (1993), Heinrich events: Chronology and processes, east-central Laurentide ice sheet and NW Labrador Sea, in *Ice in the Climate System*, *NATO ASI Ser., Ser. I*, vol. 12, edited by W. R. Peltier, pp. 167–186, Springer, New York.

Andrews, J. T., H. Erlenkeuser, K. Tedesco, A. E. Aksu, and A. J. T. Jull (1994), Late Quaternary (stage 2 and 3) meltwater and Heinrich events, northwest Labrador Sea, *Quat. Res.*, *41*, 26–34, doi:10.1006/qres.1994.1003.

Bard, E., F. Rostek, J.-L. Turon, and S. Gendreau (2000), Hydrological impact of Heinrich events in the subtropical northeast Atlantic, *Science*, *289*, 1321–1324, doi:10.1126/science.289.5483.1321.

Bassinot, F. C., L. D. Labeyrie, E. Vincent, X. Quidelleur, N. J. Shackleton, and Y. Lancelot (1994), The astronomical theory of climate and the age of the Brunhes-Matuyama magnetic reversal, *Earth Planet. Sci. Lett.*, *126*, 91–108, doi:10.1016/0012-821X(94)90244-5.

Bauch, H. A., and H. Erlenkeuser (2003), Interpreting glacial-interglacial changes in ice volume and climate from subarctic deep water foraminiferal $\delta^{18}O$, in *Earth's Climate and Orbital Eccentricity: The Marine Isotope Stage 11 Question*, *Geophys. Monogr. Ser.*, vol. 137, edited by A. W. Droxler, R. Z. Poore, and L. H. Burckle, pp. 87–102, AGU, Washington, D. C.

Biscaye, P. E. (1965), Mineralogy and sedimentation of recent deep-sea clay in the Atlantic Ocean and adjacent seas and oceans, *Geol. Soc. Am. Bull.*, *76*, 803–832, doi:10.1130/0016-7606(1965)76[803:MASORD]2.0.CO;2.

Bond, G. C., and R. Lotti (1995), Iceberg discharges into the North Atlantic on millennial time scales during the last glaciation, *Science*, *267*, 1005–1010, doi:10.1126/science.267.5200.1005.

Bond, G., et al. (1992), Evidence for massive discharges of icebergs into the North Atlantic Ocean during the last glacial period, *Nature*, *360*, 245–249, doi:10.1038/360245a0.

Bond, G. C., W. Showers, M. Elliot, M. Evans, R. Lotti, I. Hajdas, G. Bonani, and S. Johnson (1999), The North Atlantic's 1–2 kyr climate rhythm: Relation to Heinrich events, Dansgaard/Oeschger cycles and the Little Ice Age, in *Mechanisms of Global Climate Change at Millennial Time Scales*, *Geophys. Monogr. Ser.*, vol. 112, edited by P. U. Clark, R. S. Webb, and L. D. Keigwin, pp. 35–58, AGU, Washington, D. C.

Brassell, S. C., G. Eglinton, I. T. Marlowe, U. Pflaumann, and M. Sarntheim (1986), Molecular stratigraphy: A new tool for climate assessment, *Nature*, *320*, 129–133, doi:10.1038/320129a0.

Broecker, W. S. (1994), Massive iceberg discharges as triggers for global climate change, *Nature*, *372*, 421–424, doi:10.1038/372421a0.

Broecker, W. S., and J. van Donk (1970), Insolation changes, ice volumes, and the O^{18} record in deep-sea cores, *Rev. Geophys.*, *8*, 169–198, doi:10.1029/RG008i001p00169.

Broecker, W. S., G. Bond, M. Klass, E. Clark, and J. McManus (1992), Origin of the northern Atlantic's Heinrich events, *Clim. Dyn.*, *6*, 265–273, doi:10.1007/BF00193540.

Calvo, E., J. Villanueva, J. O. Grimalt, A. Boelaert, and L. Labeyrie (2001), New insights into the glacial latitudinal temperature gradients in the North Atlantic: Results from $U^{K'}_{37}$ sea surface temperatures and terrigenous inputs, *Earth Planet. Sci. Lett.*, *188*, 509–519, doi:10.1016/S0012-821X(01)00316-8.

Calvo, E., C. Pelejero, and G. A. Logan (2003), Pressurized liquid extraction of selected molecular biomarkers in deep sea sediments used as proxies in paleoceanography, *J. Chromatogr. A*, *989*(2), 197–205, doi:10.1016/S0021-9673(03)00119-5.

Channell, J. E. T., T. Kanamatsu, T. Sato, R. Stein, C. A. Alvarez Zarikian, M. J. Malone, and Expedition 303/306 Scientists (2006), *Proceedings of the Integrated Ocean Drilling Program, Volume 303/306 Expedition Reports, North Atlantic Climate*, doi:10.2204/iodp.proc.303306.2006, Integr. Ocean Drill. Program, College Station, Tex.

Conte, M. H., G. Eglinton, and L. A. S. Madureira (1992), Long-chain alkenones and alkyl alkenoates as palaeotemperature indicators: Their production, flux and early sedimentary diagenesis in the eastern North Atlantic, *Org. Geochem.*, *19*, 287–298, doi:10.1016/0146-6380(92)90044-X.

de Abreu, L., N. J. Shackleton, J. Schönfeld, M. Hall, and M. Chapman (2003), Millennial-scale oceanic climate variability off the western Iberian margin during the last two glacial periods, *Mar. Geol.*, *196*, 1–20, doi:10.1016/S0025-3227(03)00046-X.

Dowdeswell, J. A., M. A. Maslin, J. T. Andrews, and I. N. McCave (1995), Iceberg production, debris rafting, and the extent and thickness of Heinrich layers (H-1, H-2) in North Atlantic sediments, *Geology*, *23*, 301–304, doi:10.1130/0091-7613(1995)023<0297:IPDRAT>2.3.CO;2.

Expedition Scientists (2005), North Atlantic climate 2, *Prelim. Rep. 306*, doi:10.2204/IODP.PR.306.2005, Integr. Ocean Drill. Program, College Station, Tex.

Grousset, F. E., L. Labeyrie, J. A. Sinko, M. Cremer, G. Bond, J. Duprat, E. Cortijo, and S. Huon (1993), Patterns of ice-rafted detritus in the glacial North Atlantic (40–55°N), *Paleoceanography*, *8*, 175–192, doi:10.1029/92PA02923.

Gwiazda, R. H., S. R. Hemming, and W. S. Broecker (1996), Provenance of icebergs during Heinrich event 3 and the contrast to their sources during other Heinrich episodes, *Paleoceanography*, *11*, 371–378, doi:10.1029/96PA01022.

Hefter, J. (2008), Analysis of alkenone unsaturation indices with fast gas chromatography/time-of-flight mass spectrometry, *Anal. Chem.*, *80*(6), 2161–2170, doi:10.1021/ac702194m.

Hefter, J., R. Stein, and J. S. Sinninghe Damsté (2007), The biomarker inventory, trace, and source of Heinrich events and Heinrich-type layers (MIS 8–16) in the North Atlantic, *Eos Trans. AGU*, *88*(52), Fall Meet. Suppl., Abstract PP41C-0689.

Heinrich, H. (1988), Origin and consequences of cyclic ice rafting in the northeast Atlantic Ocean during the past 130,000 years, *Quat. Res.*, *29*, 142–152, doi:10.1016/0033-5894(88)90057-9.

Hemming, S. R. (2004), Heinrich events: Massive late Pleistocene detritus layers of the North Atlantic and their global climate imprint, *Rev. Geophys.*, *42*, RG1005, doi:10.1029/2003RG000128.

Hodell, D. A., J. E. T. Channell, J. H. Curtis, O. E. Romero, and U. Röhl (2008), Onset of "Hudson Strait" Heinrich events in the eastern North Atlantic at the end of the middle Pleistocene transition (~640 ka)?, *Paleoceanography*, *23*, PA4218, doi:10.1029/2008PA001591.

Huon, S., and P. Ruch (1992), Mineralogical, K-Ar and $^{87}Sr/^{86}Sr$ isotope studies of Holocene and late glacial sediments in a deep-sea core from the northeast Atlantic Ocean, *Mar. Geol.*, *107*, 275–282, doi:10.1016/0025-3227(92)90076-T.

Kirby, M. E., and J. T. Andrews (1999), Mid-Wisconsin Laurentide ice sheet growth and decay: Implications for Heinrich events 3 and 4, *Paleoceanography*, *14*, 211–223, doi:10.1029/1998PA900019.

Kissel, C., C. Laj, L. Labeyrie, T. Dokken, A. Voelker, and D. Blamart (1999), Rapid climatic variations during marine isotopic stage 3: Magnetic analysis of sediments from Nordic Seas and North Atlantic, *Earth Planet. Sci. Lett.*, *171*, 489–502, doi:10.1016/S0012-821X(99)00162-4.

Kolla, V., P. E. Biscaye, and A. F. Hanley (1979), Distribution of quartz in Late Quaternary Atlantic sediments in relation to climate, *Quat. Res.*, *11*, 261–277, doi:10.1016/0033-5894(79)90008-5.

Laskar, J., P. Robutel, F. Joutel, M. Gastineau, A. C. M. Correia, and B. Levrard (2004), A long-term numerical solution for the insolation quantities of the Earth, *Astron. Astrophys.*, *428*, 261–285, doi:10.1051/0004-6361:20041335.

Leinen, M., D. Cweink, G. R. Heath, P. E. Biscaye, V. R. Kolla, J. Thiede, and J. P. Dauphin (1986), The distribution of quartz and biogenic silica in recent deep-sea sediments, *Geology*, *14*, 199–203, doi:10.1130/0091-7613(1986)14<199:DOBSAQ>2.0.CO;2.

Lisiecki, L. E., and M. E. Raymo (2005), A Pliocene-Pleistocene stack of 57 globally distributed benthic $\delta^{18}O$ records, *Paleoceanography*, *20*, PA1003, doi:10.1029/2004PA001071.

Locarnini, R. A., A. V. Mishonov, J. I. Antonov, T. P. Boyer, and H. E. Garcia (2006), *World Ocean Atlas 2005*, vol. 1, *Temperature*, *NOAA Atlas NESDIS*, vol. 61, edited by S. Levitus, 182 pp., NOAA, Silver Spring, Md.

Madureira, L. A. S., S. A. van Kreveld, G. Eglinton, M. H. Conte, G. Ganssen, J. E. van Hinte, and J. J. Ottens (1997), Late Quaternary high-resolution biomarker and other sedimentary climate proxies in a northeast Atlantic core, *Paleoceanography*, *12*, 255–269, doi:10.1029/96PA03120.

Marlowe, I. T., S. C. Brassell, G. Eglinton, and J. C. Green (1984), Long chain unsaturated ketones and esters in living algae and marine sediments, *Org. Geochem.*, *6*, 135–141, doi:10.1016/0146-6380(84)90034-2.

Marlowe, I. T., S. C. Brassell, G. Eglinton, and J. C. Green (1990), Long-chain alkenones and alkyl alkenoates and the fossil coccolith record of marine sediments, *Chem. Geol.*, *88*, 349–375, doi:10.1016/0009-2541(90)90098-R.

Martrat, B., J. O. Grimalt, N. J. Shackleton, L. de Abreu, M. A. Hutterli, and T. F. Stocker (2007), Four climate cycles of recurring deep and surface water destabilizations on the Iberian margin, *Science*, *317*, 502–507, doi:10.1126/science.1139994.

Maslin, M. A., N. J. Shackleton, and U. Pflaumann (1995), Surface water temperature, salinity, and density changes in the northeast Atlantic during the last 45,000 years: Heinrich events, deep water formation, and climate rebounds, *Paleoceanography*, *10*, 527–544, doi:10.1029/94PA03040.

McManus, J. F., R. F. Anderson, W. S. Broecker, M. Q. Fleisher, and S. M. Higgins (1998), Radiometrically determined sedimentary fluxes in the sub-polar North Atlantic during the last 140,000 years, *Earth Planet. Sci. Lett.*, *155*, 29–43, doi:10.1016/S0012-821X(97)00201-X.

McManus, J. F., D. W. Oppo, and J. L. Cullen (1999), A 0.5-million-year record of millennial-scale climate variability in the North Atlantic, *Science*, *283*, 971–975, doi:10.1126/science.283.5404.971.

Moros, M., A. Kuijpers, I. Snowball, S. Lassen, D. Bäckström, F. Gingele, and J. F. McManus (2002), Were glacial iceberg surges in the North Atlantic triggered by climatic warming?, *Mar. Geol.*, *192*, 393–417, doi:10.1016/S0025-3227(02)00592-3.

Moros, M., J. McManus, T. Rasmussen, A. Kuijpers, T. Dokken, I. Snowball, T. Nielsen, and E. Jansen (2004), Quartz content and the quartz-to-plagioclase ratio determined by X-ray diffraction: A proxy for ice rafting in the northern North Atlantic?, *Earth Planet. Sci. Lett.*, *218*, 389–401, doi:10.1016/S0012-821X(03)00675-7.

Müller, P. J., G. Kirst, G. Ruhland, I. von Storch, and A. Rosell-Melé (1998), Calibration of the alkenone paleotemperature index $U^{K'}_{37}$ based on core-tops from the eastern South Atlantic and the global ocean (60°N–60°S), *Geochim. Cosmochim. Acta*, *62*(10), 1757–1772, doi:10.1016/S0016-7037(98)00097-0.

Nave, S., L. Labeyrie, J. Gherardi, N. Caillon, E. Cortijo, C. Kissel, and F. Abrantes (2007), Primary productivity response to Heinrich events in the North Atlantic Ocean and Norwegian Sea, *Paleoceanography*, *22*, PA3216, doi:10.1029/2006PA001335.

Oppo, D. W., J. F. McManus, and J. L. Cullen (1998), Abrupt climate events 500,000 to 340,000 years ago: Evidence from subpolar North Atlantic sediments, *Science*, *279*, 1335–1338, doi:10.1126/science.279.5355.1335.

Pflaumann, U., et al. (2003), Glacial North Atlantic: Sea-surface conditions reconstructed by GLAMAP 2000, *Paleoceanography*, *18*(3), 1065, doi:10.1029/2002PA000774.

Prahl, F. G., and L. A. Muehlhausen (1989), Lipid biomarkers as geochemical tools for paleoceanographic study, in *Productivity of the Ocean: Present and Past*, *Life Sci. Res. Rep.*, vol. 44, edited by W. H. Berger et al., pp. 271–290, Wiley-Interscience, Chichester, U. K.

Prahl, F. G., and S. G. Wakeham (1987), Calibration of unsaturation patterns in long-chain ketone compositions for paleotemperature assessment, *Nature*, *330*, 367–369, doi:10.1038/330367a0.

Rashid, H., and E. Grosjean (2006), Detecting the source of Heinrich layers: An organic geochemical study, *Paleoceanography*, *21*, PA3014, doi:10.1029/2005PA001240.

Rashid, H., R. Hesse, and D. J. W. Piper (2003), Distribution, thickness and origin of Heinrich layer 3 in the Labrador Sea, *Earth Planet. Sci. Lett.*, *205*, 281–293, doi:10.1016/S0012-821X(02)01047-6.

Raymo, M. E. (1992), Global climate change: A three million year perspective, in *Start of a Glacial*, *NATO ASI Ser., Ser. I*, vol. 3, edited by G. J. Kukla and E. Went, pp. 207–223, Springer, Heidelberg, Germany.

Raymo, M. E., W. F. Ruddiman, J. Backman, B. M. Clement, and D. G. Martinson (1989), Late Pliocene variation in Northern Hemisphere ice sheets and North Atlantic deep water circulation, *Paleoceanography*, *4*, 413–446, doi:10.1029/PA004i004p00413.

Robinson, S. G., M. A. Maslin, and I. N. McCave (1995), Magnetic susceptibility variations in Upper Pleistocene deep-sea sediments of the NE Atlantic: Implications for ice rafting and paleocirculation at the Last Glacial Maximum, *Paleoceanography*, *10*, 221–250, doi:10.1029/94PA02683.

Rosell-Melé, A. (1998), Interhemispheric appraisal of the value of alkenone indices as temperature and salinity proxies in high-latitude locations, *Paleoceanography*, *13*, 694–703, doi:10.1029/98PA02355.

Rosell-Melé, A. (2001), Examination of the use of biomarker proxies for the reconstruction of paleoceanographic conditions in the northern North Atlantic, in *The Northern North Atlantic: A Changing Environment*, edited by P. Schäfer et al., pp. 353–363, Springer, Heidelberg, Germany.

Rosell-Melé, A., M. A. Maslin, J. R. Maxwell, and P. Schaeffer (1997), Biomarker evidence

for "Heinrich" events, *Geochim. Cosmochim. Acta*, *61*(8), 1671–1678, doi:10.1016/S0016-7037(97)00046-X.

Rosell-Melé, A., E. Jansen, and M. Weinelt (2002), Appraisal of a molecular approach to infer variations in surface ocean freshwater inputs into the North Atlantic during the last glacial, *Global Planet. Change*, *34*(3–4), 143–152, doi:10.1016/S0921-8181(02)00111-X.

Ruddiman, W. F. (1977), North Atlantic ice-rafting: A major change at 75,000 years before the present, *Science*, *196*, 1208–1211, doi:10.1126/science.196.4295.1208.

Ruddiman, W. F., et al. (1987), *Initial Reports of the Deep Sea Drilling Project*, vol. 94, U.S. Govt. Print. Off., Washington, D. C.

Ruddiman, W. F., M. E. Raymo, D. G. Martinson, B. M. Clement, and J. Backman (1989), Pleistocene evolution: Northern Hemisphere ice sheets and North Atlantic Ocean, *Paleoceanography*, *4*, 353–412, doi:10.1029/PA004i004p00353.

Sarnthein, M., G. Tetzlaff, B. Koopmann, K. Wolter, and U. Pflaumann (1981), Glacial and interglacial wind regimes over the eastern subtropical Atlantic and northwest Africa, *Nature*, *293*, 193–196, doi:10.1038/293193a0.

Sarnthein, M., et al. (2001), Fundamental modes and abrupt changes in North Atlantic circulation and climate over the last 60 ky—Concepts, reconstruction and numerical modeling, in *The Northern North Atlantic: A Changing Environment*, edited by P. Schäfer et al., pp. 365–410, Springer, Heidelberg, Germany.

Sarnthein, M., R. Gersonde, S. Niebler, U. Pflaumann, R. Spielhagen, J. Thiede, G. Wefer, and M. Weinelt (2003), Overview of Glacial Atlantic Ocean Mapping (GLAMAP 2000), *Paleoceanography*, *18*(2), 1030, doi:10.1029/2002PA000769.

Shackleton, N. J. (1974), Attainment of isotopic equilibrium between ocean water and the benthonic foraminifera genus *Uvigerina*: Isotopic changes in the ocean during the last glacial, *Colloq. Int. C. N. R. S.*, *219*, 203–209.

Shackleton, N. J. (1987), Oxygen isotopes, ice volume and sea level, *Quat. Sci. Rev.*, *6*, 183–190, doi:10.1016/0277-3791(87)90003-5.

Sicre, M.-A., E. Bard, U. Ezat, and F. Rostek (2002), Alkenone distributions in the North Atlantic and Nordic sea surface waters, *Geochem. Geophys. Geosyst.*, *3*(2), 1013, doi:10.1029/2001GC000159.

Stein, R., et al. (2006), North Atlantic paleoceanography: The last five million years, *Eos Trans. AGU*, *87*(13), doi:10.1029/2006EO130002.

Stoner, J. S., J. E. T. Channell, and C. Hillaire-Marcel (1996), The magnetic signature of rapidly deposited detrital layers from the deep Labrador Sea: Relationship to North Atlantic Heinrich layers, *Paleoceanography*, *11*, 309–325, doi:10.1029/96PA00583.

van Andel, T. H., G. H. Heath, and T. C. Moore Jr. (1975), Cenozoic history and paleoceanography of the central equatorial Pacific, *Mem. Geol. Soc. Am.*, *143*, 134 pp.

van Kreveld, S. A., M. Knappertsbusch, J. Ottens, G. M. Ganssen, and J. E. van Hinte (1996), Biogenic carbonate and ice-rafted debris Heinrich layer accumulation in deep-sea sediments from a northeast Atlantic piston core, *Mar. Geol.*, *131*, 21–46, doi:10.1016/0025-3227(95)00143-3.

Villanueva, J., J. O. Grimalt, E. Cortijo, L. Vidal, and L. Labeyrie (1997), A biomarker approach to the organic matter deposited in the North Atlantic during the last climatic cycle, *Geochim. Cosmochim. Acta*, *61*(21), 4633–4646, doi:10.1016/S0016-7037(97)83123-7.

Villanueva, J., E. Calvo, C. Pelejero, J. O. Grimalt, A. Boelaert, and L. Labeyrie (2001), A latitudinal productivity band in the central North Atlantic over the last 270 kyr: An alkenone perspective, *Paleoceanography*, *16*, 617–626, doi:10.1029/2000PA000543.

Volkman, J. K., G. Eglinton, E. D. S. Corner, and J. R. Sargent (1980), Novel unsaturated straight-chain C_{37}–C_{39} methyl and ethyl ketones in marine sediments and a coccolithophore *Emiliania huxleyi*, in *Advances in Organic Geochemistry, 1979*, edited by A. G. Douglas and J. R. Maxwell, pp. 219–228, Pergamon, Oxford, U. K.

Wright, A. K., and B. P. Flower (2002), Surface and deep ocean circulation in the subpolar North Atlantic during the mid-Pleistocene revolution, *Paleoceanography*, *17*(4), 1068, doi:10.1029/2002PA000782.

J. Grützner, Center for Marine Environmental Sciences, Bremen University, D-28334 Bremen, Germany.

J. Hefter, B. D. A. Naafs, and R. Stein, Alfred Wegener Institute for Polar and Marine Research, D-27568 Bremerhaven, Germany. (ruediger.stein@awi.de)

A. Voelker, Departamento Geologia Marinha, LNEG, P-2721-866 Alfragide, Portugal.